Conformational and Thermodynamic Control of Electron Transfer in Neuronal Nitric Oxide Synthase†

Adrian J. Dunford,‡ Stephen E. J. Rigby,§ Sam Hay,‡ Andrew W. Munro,|| and Nigel S. Scrutton*,‡

Faculty of Life Sciences, Manchester Interdisciplinary Biocentre, University of Manchester, 131 Princess Street, Manchester M1 7DN, U.K., School of Biological and Chemical Sciences, Queen Mary College, University of London, London E1 4NS, U.K., and School of Chemical Engineering and Analytical Science, Manchester Interdisciplinary Biocentre, University of Manchester, 131 Princess Street, Manchester M1 7DN, U.K.

Received January 24, 2007; Revised Manuscript Received March 5, 2007

ABSTRACT: Multiple solution-state techniques have been employed in investigating the nature and control of electron transfer in the context of the proposed "domain shuffle hypothesis" for intraprotein electron transfer inferred from the crystal structure of the nitric oxide synthase reductase domain. NADPH analogues and fragments have been used to map those regions of this substrate that are important in eliciting a conformational change, observed in both the fluorescence emission of the flavin cofactors of the enzyme and the EPR spectra of the FMN flavosemiquinone state. EPR and UV−visible potentiometric methods have demonstrated a substantial calmodulin-dependent perturbation in the midpoint reduction potentials of the redox couples of both flavin cofactors, in contrast to a previous report [Noble, M. A., et al. (1999) *Biochemistry 38*, 16413−16418]. These studies support a model in which FMN domain mobility, triggered by Ca^{2+}−calmodulin binding and antagonized by substrate binding, facilitates electron transfer in nitric oxide synthase through conformational change and effects a major change in the midpoint reduction potentials of the flavin redox couples. These results are discussed in light of the recent crystal structure of the NADPH-locked reductase domain.

Nitric oxide (NO)[1] is a transient, small, and readily diffusible molecule. It has a central role in key physiological processes, including blood pressure regulation, neurotransmission, and the immune response (*1*). Deregulation of its synthesis contributes to a number of human pathologies, including stroke, inflammatory bowel disease, immune-type diabetes, rheumatoid arthritis, hypertension, arteriosclerosis, and susceptibility to infection (*2*). The production of NO is mediated by the nitric oxide synthase (NOS) enzymes that utilize NADPH as an electron source to catalyze the oxygen-dependent conversion of L-arginine to L-citrulline and nitric oxide (NO) (*3*−*5*). NOSs are dimeric flavoheme enzymes, and each monomer comprises a C-terminal diflavin reductase domain and an N-terminal oxygenase domain (*6*−*9*). The reductase domain is related to cytochrome P450 reductase (CPR) (*10*, *11*), methionine synthase reductase (MSR) (*12*), and the cancer-associated protein novel reductase 1 (NR1) (*13*). The N-terminal oxygenase domain of NOS contains 1 molar equiv of heme *b* and possesses binding sites for L-arginine and (6*R*)-5,6,7,8-tetrahydrobiopterin (*14*). Of the three NOS isoforms, the inducible NOS isoform is expressed with CaM tightly bound (*15*), and regulation of activity is primarily through transcriptional processes; the activities of endothelial NOS (eNOS) and neuronal NOS (nNOS) are regulated by CaM binding, which in turn is controlled by intracellular calcium levels (*6*−*8*) and is mediated by an autoinhibitory helix (AH) sequence in the FMN domain (*16*). The reductase and oxygenase domains are linked by a calmodulin (CaM) binding sequence (*10*, *15*, *17*, *18*), and CaM acts to facilitate electron transfer through NOS by releasing a NADPH-dependent conformational lock (*19*). CaM binding stimulates FMN-to-heme electron transfer and is also proposed to enhance the rate of interflavin electron transfer in the reductase domain (*20*−*22*), although direct assessment of the effects of CaM on individual steps in the electron transfer mechanism of the reductase domain is compromised by the multiple kinetic phases observed in stopped-flow studies (*23*). Enhanced steady-state rates of cytochrome *c* reduction by NOS reductase effected by CaM binding are attributed mainly to faster FMN-to-cytochrome *c* electron transfer rates in the presence of CaM, through release of the NADPH-dependent conformational lock (*19*). While the presence of the heme domain in full-length nNOS does lead to some changes in kinetic parameters for cytochrome *c* reduction, the key factor here is that CaM binding

† The work was funded by the UK Biotechnology and Biological Sciences Research Council. N.S.S. is a BBSRC Professorial Research Fellow.

* To whom correspondence should be addressed. Telephone: +44 1613065152. Fax: +441613068918. E-mail: nigel.scrutton@manchester.ac.uk.

‡ Manchester Interdisciplinary Biocentre, Faculty of Life Sciences, University of Manchester.

§ University of London.

|| Manchester Interdisciplinary Biocentre, School of Chemical Engineering and Analytical Science, University of Manchester.

[1] Abbreviations: 2′-AMP, 2′-adenosine monophosphate; 3′-AMP, 3′-adenosine monophosphate; 5′-AMP, 5′-adenosine monophosphate; 2′,5′-ADP, 2′,5′-adenosine diphosphate; CaM^+, calmodulin-bound; CaM^-, calmodulin-free; CPR, cytochrome P450 reductase; E_M, midpoint reduction potential; EPR, electron paramagnetic resonance; ΔH_{pp}, line width; hq, hydroquinone; NMN, nicotinamide mononucleotide; nNOS, neuronal nitric oxide synthase; $nNOS_{RED}$, neuronal nitric oxide synthase reductase domain; ox, oxidized; red, reduced; sq, semiquinone.

10.1021/bi7001339 CCC: $37.00
Published on Web 04/06/2007

to the nNOS reductase effects a 10-fold enhancement in the cytochrome *c* reduction rate, as previously reported for both the reductase and the full-length enzyme (*24*). The reductase domain is catalytically functional as a NADPH-dependent cytochrome *c* reductase, and the effects of CaM are complete within the reductase domain and are manifest as enhancements of steady-state reactivity with cytochrome *c* (similar in magnitude to those seen for the intact nNOS in NO production).

The crystal structure of the isolated FAD domain (*25*) and the reductase domain ($nNOS_{RED}$) of rat nNOS (*26*) provides a framework for developing models of electron transfer and the role of regulatory elements. The reductase domain comprises four major domains: the FMN-binding domain (residues 750−942), the connecting domain (residues 943−989 and 1039−1170) with a flexible hinge (residues 943−967) and a β-finger (residues 1059−1078), a FAD-binding domain (residues 990−1038 and 1171−1231), and a NADPH-binding domain (residues 1232−1396). The "domain shuffle hypothesis" for electron transfer invokes a mobile FMN-binding domain to shuttle electrons from the FAD to the heme of the oxygenase domain in the second subunit of the enzyme dimer (*26*). In the crystal structure of $nNOS_{RED}$ (i.e., the NADPH-locked enzyme in the absence of CaM), the negatively charged 2′-phosphate group of NADPH interacts with residue Arg-1400 of the C-terminal tail (CT) regulatory region. This mode of binding represses CaM activation of electron transfer in NOS, consistent with the kinetically observed NADPH lock (*19*). The AH regulatory insert (residues 840−848) of the FMN domain interacts with the NADPH-binding domain and FMN domain and contains a canonical CaM-binding sequence and site for phosphorylation (Ser-847). In the domain shuffle hypothesis, binding of CaM to both the AH region and the CaM-binding linker between the reductase and oxygenase domains is proposed to release the FMN domain from its locked position seen in the crystal structure of $nNOS_{RED}$, thereby facilitating interdomain electron transfer (*26*). Additionally, the helical CT region (residues 1401−1412) is accommodated within a negatively charged groove across the FMN−FAD domain interface where it represses electron transfer. The CT region includes Arg-1400 that interacts with the 2′-phosphate of NADPH and is terminated by Ser-1412 (a site of phosphorylation). Interactions of the CT region with the FMN and NADPH-binding domains "lock" the FMN domain into a position in which it can accept electrons readily from the FAD domain. In this position, negatively charged residues of the FMN domain (comprising residues Glu-916 and Asp-918) surround Ser-1412. It has been suggested that phosphorylation of Ser-1412 would induce conformational change through electrostatic interaction, unlocking the arrangement observed in the crystal structure and thereby contributing to increased domain flexibility in the $nNOS_{RED}$ domain (*26*).

Herein, we employ multiple solution-state techniques to provide strong evidence for a calmodulin-dependent change in the midpoint reduction potentials of nNOS reductase, contrary to a previous report (*27*). We also provide solution data that are consistent with the proposed domain shuffle hypothesis for electron transfer in nNOS, inferred from the crystallographic structure of nNOS reductase.

MATERIALS AND METHODS

Materials. Cytochrome *c*, 2′-AMP, 3′-AMP, 5′-AMP, 2′,5′-ADP, and NMN were purchased from Sigma (Poole, U.K.). $NADP^+$ and NAD^+ were purchased from Melford (Ipswich, U.K.). All other reagents were purchased from Sigma and were of the highest available grade.

Purification of the nNOS Reductase Domain. Escherichia coli strain BL21(DE3) transformed with plasmid pCRNNR was grown in Terrific Broth, and expression of the reductase domain (residues 695−1429 that encompass the calmodulin binding linker region) was induced by addition of isopropyl thio-β-D-galactoside (1 mM), essentially as described previously (*23*). Harvested cells were resuspended in lysis buffer [50 mM Tris-HCl (pH 7.4) containing 10% (v/v) glycerol, 1 mM $CaCl_2$, and a Complete EDTA-free protease inhibitor tablet (Roche)]. Cells were disrupted by sonication, and the cell extract was clarified by centrifugation (18000*g* for 30 min). Enzyme was applied to an affinity resin (2′5′-ADP Sepharose) equilibrated with lysis buffer containing 100 mM NaCl. After the sample was washed [∼250 mL of lysis buffer (100 mM NaCl) and then ∼250 mL of lysis buffer (250 mM NaCl)], CaM-bound reductase domain was recovered by the application of lysis buffer containing 1 M NaCl with 25 mM 2′-AMP. Enzyme was dialyzed against lysis buffer and concentrated before being applied to a hydroxyapatite column pre-equilibrated with lysis buffer. After the sample was washed with lysis buffer, the reductase domain was eluted using a gradient of 0 to 500 mM KCl. Enzyme was dialyzed exhaustively against lysis buffer and stored at −80 °C in the presence of 20% (v/v) glycerol. The presence of CaM and the lack of proteolysis of the $nNOS_{RED}$ were demonstrated as described previously (*23*). The enzyme concentration was determined spectrophotometrically (ϵ_{454} = 21 600 M^{-1} cm^{-1}) (*27*).

Steady-State Enzyme Assays. Steady-state activities of $nNOS_{RED}$ in the presence and absence of CaM and using cytochrome *c* as an electron acceptor were determined using a Varian Cary UV-50 Bio UV−visible spectrophotometer. Cytochrome *c* (horse heart) reduction was assessed at 550 nm [$\Delta\epsilon_{550(red-ox)}$ = 22 640 M^{-1} cm^{-1}] (*28*). Reactions were performed in 50 mM Tris-HCl (pH 7.4) containing 10% (v/v) glycerol at 25 °C. Studies involving $nNOS_{RED}$ CaM^+ had 1 mM $CaCl_2$ present in the buffer, whereas studies involving $nNOS_{RED}$ CaM^- contained 1 mM EGTA. The steady-state activity with cytochrome *c* as the electron acceptor was used as a reference to demonstrate the expected 10-fold difference between the activities of the CaM-bound and CaM-free forms of nNOS reductase (*20*, *24*, *29*, *30*). Determined k_{cat} and K_m values were within error of those published by Gachhui et al. (*24*) and Knight and Scrutton (*23*). Once the 10-fold stimulation by CaM was established, inhibition studies were performed to determine the K_i values with nucleotide analogues for both the CaM-bound and CaM-free forms of $nNOS_{RED}$. Values for K_i were determined by fitting data to the appropriate equation using Origin (Microcal). For inhibition studies, nNOS in the CaM-bound and CaM-free states and cytochrome c^{3+} were used at a concentration of 10 nM and 10 μM, respectively. The concentration of $NADP^+$ and analogues was varied over the range of 0−2.5 mM. Enzyme was incubated with ligand for sufficient time prior to initiation of the reaction to allow for complete equilibration

of NOS structure (see Figure 2). Assays were initiated by microliter additions of NADPH at final concentrations of 1, 10, and 100 μM at 25 °C. Data were analyzed using the Dixon plot (*31*).

Fluorescence Assays. Fluorescence studies were performed on a Varian Cary Eclipse fluorescence spectrophotometer at 25 °C in 100 mM Tris-HCl (pH 7.4) and 10% (v/v) glycerol. $nNOS_{RED}$ CaM^+ contained 1 mM $CaCl_2$, while $nNOS_{RED}$ CaM^- contained 1 mM EGTA. The $nNOS_{RED}$ (4 μM) was mixed with the nucleotide analogues 2′-AMP, 3′-AMP, 5′-AMP, 2′,5′-ADP, NMN, $NADP^+$, or NAD^+, and the subsequent change in fluorescence was monitored over the wavelength range of 470−800 nm. The excitation wavelength was 453 nm.

Spectroelectrochemical Redox Potentiometry. Redox titrations were performed in a Belle Technology glovebox under a dinitrogen atmosphere, maintained at less than 2 ppm oxygen. All buffers and solutions were degassed by being bubbled with argon prior to entering the glovebox to ensure removal of all traces of dioxygen. The protein was applied to a Pharmacia PD-10 desalting column in the anaerobic box, pre-equilibrated with degassed 100 mM Tris-HCl buffer (pH 7.4) 10% (v/v) glycerol (titration buffer), to ensure removal of all traces of oxygen. The protein solutions were titrated electrochemically according to the method of Dutton (*32*) using sodium dithionite as the reductant and potassium ferricyanide as the oxidant. Titrations were performed in both reductive and oxidative directions to ensure a lack of hysteresis. Dithionite and ferricyanide were delivered in approximately 2 μL aliquots from concentrated stock solutions (typically 10−50 mM). Mediators were added to facilitate electrical communication between enzyme and electrode, prior to titration. Phenazine methosulfate (2 μM), 2-hydroxy-1,4-naphthoquinone (5 μM), methyl viologen (0.5 μM), and benzyl viologen (1 μM) were included to mediate in the range from 100 to −480 mV, as described previously (*33*). The electrode was allowed to stabilize between each addition. Spectra (300−800 nm) were recorded using a Cary UV-50 Bio UV−visible scanning spectrophotometer. The electrochemical potential of the solution was measured using a Hanna pH 211 meter coupled to a Pt/Calomel electrode (ThermoRussell Ltd.) at 25 ± 2 °C. The electrode was calibrated using the Fe^{3+}/Fe^{2+} EDTA couple as a standard (108 mV). A factor of 244 mV was used to correct relative to the standard hydrogen electrode. Data manipulation and analysis were performed using Origin (Microcal). For titration of the nNOS reductase domain, absorbance values at 456 nm (near the absorption maximum for the oxidized flavins in both CaM-free and CaM-bound $nNOS_{RED}$) and 592 nm (near the absorption maximum for the blue semiquinone form of the flavins) were plotted against the applied potential. Analyses were also conducted at both 507 nm (apparent isosbestic point for the flavin oxidized−semiquinone couples) and 416 nm (isosbestic for flavin semiquinone−hydroquinone couples) to obtain approximations of the opposite redox couples. As reported previously, data at 456 and 592 nm were fitted to eqs 1 and 2, respectively. Equation 1 represents a four-electron redox process occurring in sequential one-electron steps, while eq 2 is a composite of two separate two-electron terms and is used to fit the bell-shaped curves described by absorption versus potential data at the semiquinone wavelength (592 nm). Both equations are derived by extension to the Nernst equation and the Beer−Lambert law.

$$A = \frac{a \times 10^{(2E-E_1'-E_2')/59} + b \times 10^{(E-E_2')/59} + c + d \times 10^{(E_3'-E)/59} + e \times 10^{(E_3'+E_4'-2E)/59}}{1 + 10^{(2E-E_1'-E_2')/59} + 10^{(E-E_2')/59} + 10^{(E_3'-E)/59} + 10^{(E_3'+E_4'-2E)/59}} \quad (1)$$

where A is the total absorbance and $a-e$ are the relative absorbance values contributed by the two flavins in each of five nondegenerate oxidation states. E_1', E_2', E_3', and E_4' are the four midpoint potentials, two for each flavin.

$$A = \frac{a \times 10^{(E-E_1')/59} + b + c \times 10^{(E_2'-E)/59}}{1 + 10^{(E-E_1')/59} + 10^{(E_2'-E)/59}} + \frac{d \times 10^{(E-E_3')/59} + e + f \times 10^{(E_4'-E)/59}}{1 + 10^{(E-E_3')/59} + 10^{(E_4'-E)/59}} \quad (2)$$

where A is the total absorbance, a, b, and c are component absorbance values contributed by a flavin in the oxidized, semiquinone, and reduced states, respectively, d, e, and f are component absorbance values contributed by the other flavin, and E is the observed potential. E_1', E_2', E_3', and E_4' are the midpoint potentials for oxidized−semiquinone and semiquinone−reduced couples, respectively.

Optical potentiometry spectroscopy experiments were also analyzed by global analysis using SpecFit/32 (Bio-Logic Science Instruments, Grenoble, France). Potentials were determined, and spectra deconvoluted, using a Nernstian model with five species and four $n = 1$ potentials: a ↔ b ↔ c ↔ d ↔ e. In the case of the CaM-free data, the model was modified, a ↔ b ← ($n = 2$) → d ↔ e, as species c (FAD^-, FMN^-) was not resolved, presumably due to the much smaller overlap of the FAD E_1' and FMN E_2' potentials.

Electron Paramagnetic Resonance Spectroscopy. During the spectroelectrochemical titrations with dithionite (see above), samples (200 μL) of enzyme were withdrawn for EPR spectroscopic analysis. The samples were placed in standard 3 mm quartz EPR tubes and sealed with Parafilm inside the glovebox, where they were immediately removed and frozen in liquid nitrogen. Samples were stored in liquid nitrogen to prevent reoxidation until they were analyzed. EPR spectra were recorded on a Bruker ELEXSYS E500 spectrometer fitted with an Oxford Instruments ESR900 liquid helium cryostat. Solution conditions were as given for the redox potentiometry described above. The concentration of $nNOS_{RED}$ was 64 μM in the CaM-bound samples and 53 μM in the CaM-free samples used in the redox titration shown. The $nNOS_{RED}$ concentration employed for the $NADP^+$ fragment binding studies was 112 μM. The flavosemiquinone concentration was estimated by double integration relative to a 100 μM sample of Cu-EDTA, the spectrum of the latter being recorded under the same conditions as the flavosemiquinone spectra. Midpoint potentials were estimated from these experiments by fitting these data to eq 3 in a fashion similar to that for the absorbance data.

$$I = a[1 + 10^{(E-E_1')/59} + 10^{(E_2'-E)/59}]^{-1} + a[1 + 10^{(E-E_3')/59} + 10^{(E_4'-E)/59}]^{-1} \quad (3)$$

Equation 3 differs from eqs 1 and 2 in that it treats the concentration and signal intensity of the FMN and FAD as equal, thus reducing the risk of erroneously fitting a contaminating species such as a mediator. The CaM-free data were fit with an additional term $\{b[1 + 10^{(E-E_5')/59} + 10^{(E_6'-E)/59}]^{-1}\}$ to describe the "feature" centered around 100 mV that reports the contribution from a mediator radical.

RESULTS AND DISCUSSION

Inhibition of nNOS$_{RED}$ by NADP$^+$ Analogues and Fragments. To characterize the key determinants involved in substrate binding, we performed a series of inhibition studies with NADP$^+$ fragments. Steady-state turnover analysis in the presence of different inhibitors established that NADP$^+$ and 2′,5′-ADP are potent competitive inhibitors of the transfer of electrons from nNOS$_{RED}$ to cytochrome *c* in both the CaM-free and CaM-bound forms (Table 1). Both the 2′- and 5′-phosphate groups contribute significantly to the binding affinity of the inhibitors. Removal of the 5′-phosphate group is responsible for 20-fold (nNOS$_{RED}$/CaM-bound) and 64-fold (nNOS$_{RED}$/CaM-free) increases in the K_i value for the inhibitor, which is evident from a comparison of the K_i values for 2′,5′-ADP and 2′-AMP. Likewise, removal of the 2′-phosphate group leads to 67-fold (nNOS$_{RED}$/CaM-bound) and 151-fold (nNOS$_{RED}$/CaM-free) increases in the K_i value [comparing K_i values for 2′,5′-ADP with those for 5′-AMP (Table 1)]. Both NAD$^+$ and NMN, which lack some or all of the binding determinants from the adenosine region of the natural substrate, are poor inhibitors of nNOS$_{RED}$. The data are consistent with putative key interactions made between nNOS$_{RED}$ and substrate, as inferred from the structure of the CaM-free nNOS$_{RED}$ in complex with NADP$^+$ (*26*) (Figure 1). Garcin and co-workers reported in ref *26* that the NMN portion of NADP$^+$ binds in a different position in each subunit of nNOS$_{RED}$, likely reflecting relatively weaker binding of this region of the substrate by the protein. At the adenosine end of the NADP$^+$, AN1 and AN3 of the adenosine base interact with Gln-1324 OE1 (2.7 Å) and a water molecule (2.8 Å), respectively. Interactions of the ribose sugar of the adenosine region of NADP$^+$ and its 2′-phosphate group with the protein involve a network of hydrogen bonds involving side chains, backbone atoms, and water. Ser-1313 forms hydrogen bonds involving the side chain OG atom and atoms AOP1 (2.4 Å), AO3* (2.5 Å), and AO2* (3.0 Å) of NADP$^+$. The backbone carbonyl of Cys-1283 forms a weak interaction with atom AO3* (2.9 Å) of NADP$^+$, and the NE atom of Arg-1314 interacts weakly with the AOP1 atom (2.9 Å) of NADP$^+$. Tyr-1322 OH (2.5 Å) and Arg-1400 NH2 (3.1 Å) also form interactions with the phosphate AOP2 atom. This latter interaction is consistent with mutagenesis studies (*26*, *34*) in which the interaction between Arg-1400 and the 2′-phosphate group of NADP$^+$ was eliminated. Our steady-state inhibition (Table 1) and static fluorescence studies (see below) also demonstrate the importance of those interactions between the protein and the 2′-phosphate group of the substrate; interactions with the 5′-phosphate contribute less to binding (Table 1), and phosphorylation at the nonphysiological 3′ position does not contribute significantly to improved binding. The pyrophosphate moiety also forms a number of interactions with the protein. For example, atom AO1 of the phosphate forms a hydrogen bond to Arg-1284 (2.8 Å) and atom NO5* to Arg-1010 NH2 (3.0 Å). Also, atoms NO1 and NO2 interact with water molecules (2.7 and 2.6 Å, respectively). In subunit B, two additional weak interactions are inferred between AO1 and Arg-1010 NH1 (3.0 Å) and between NO5 and Arg-1010 NH2 (2.8 Å). The NMN portion of the substrate is weakly bound. Only one putative interaction is seen between NO2* of the ribose and the backbone carbonyl of Thr-1398 (2.4 Å). The electron density of NADP$^+$ shows a large region of unoccupied density adjacent to the position of the modeled NMN portion which suggests multiple positions for these atoms. This seems likely as the NMN is not appropriately positioned for hydride transfer. The lack of extensive interaction is consistent with the less potent inhibitory properties of the NMN fragment compared with those fragments derived from the adenosine part of NADP$^+$ (Table 1). Clearly, in both subunits, the position of the NMN portion is uncertain despite the remainder of the substrate being clearly defined by the electron density (*26*). The extensive interactions of the adenosine and phosphate groups restrict the mobility of the NADP(H) as a whole, but it is likely that in solution during turnover, specific interactions are broken and formed as hydride transfer occurs. Overall, the crystal structure data support the steady-state inhibition studies in which the NMN fragment has the weakest effect on inhibition (largest K_i), due to NMN having the fewest interactions with the protein backbone. Examining the effects of the 2′-phosphate demonstrates its importance in the 2′-position rather than the 3′-position. This is supported by inhibition studies with NAD$^+$, which show that the absence of the 2′-phosphate results in an 83-fold increase in the measured K_i. The 2′,5′-ADP acts as a powerful inhibitor during steady-state turnover (almost equal to NADP$^+$ itself). Since virtually all the protein−substrate interactions are within the 2′,5′-ADP moiety of NADP$^+$, this supports the idea of the NMN fragment being mobile, as it does not bind tightly to the protein.

Table 1: Competitive Inhibition Data for Substrate (NADPH) Analogues and Structural Fragments with CaM-Bound and CaM-Free nNOS$_{RED}$[a]

analogue	CaM$^+$ nNOS (μM)	CaM$^-$ nNOS (μM)
2′-AMP	125 ± 8	450 ± 35
3′-AMP	400 ± 30	1030 ± 75
5′-AMP	400 ± 25	1060 ± 80
2′,5′-ADP	6 ± 1	7 ± 1
NMN	510 ± 35	1010 ± 70
NAD$^+$	500 ± 30	1500 ± 75
NADP$^+$	4 ± 1	7 ± 1

[a] Values are K_i constants determined as described in Materials and Methods. The data were replicated using two different preparations of the enzyme.

Static Fluorescence Assays. Fluorescence emission of the flavins was monitored following addition of NADP$^+$ and analogues to nNOS$_{RED}$. Changes in fluorescence emission were recorded over a 20 min time period, after which further fluorescence changes did not occur. Control studies, in which buffer alone was added to the protein, did not yield fluorescence changes associated with the flavin cofactors. Earlier work by Stuehr and co-workers showed that NADP$^+$

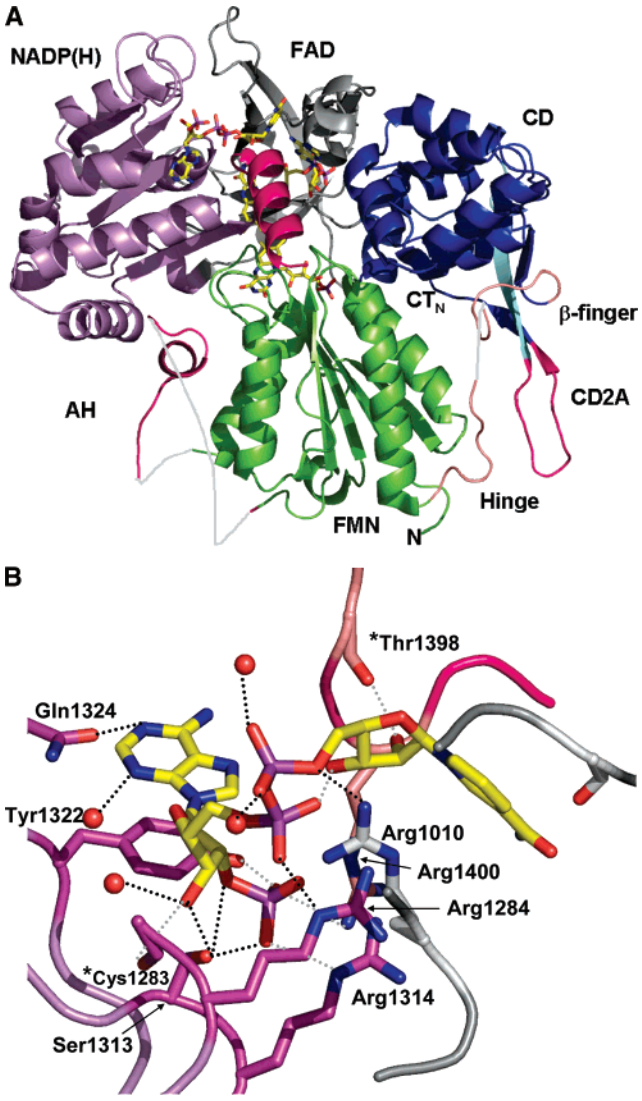

FIGURE 1: (A) Domain organization and regulatory elements in the NADP(H)-locked form of nNOS$_{RED}$. The domains are shown as cartoons while the cofactors as "atom-colored sticks". The FMN domain is colored green, the NADPH domain light purple, the FAD domain gray, and the connecting domain (CD) blue. The C-terminal region (CT$_N$), CD2A which is a CaM-binding region (the main CaM binding region is located in the N-terminal region prior to the NOS$_{red}$ domains and not shown in the structure in Figure 1), and the autoinhibitory helix (AH) are also shown. Only one subunit of the homodimer is shown. Panel A was adapted from PDB entry 1TLL (*25*). (B) Detail of the interactions made between nNOS$_{RED}$ and NADPH. The backbone trace is shown as ribbons with additional atoms shown as atom-colored sticks. Carbon atoms are colored with the same color as their respective domain in panel A. Water molecules are depicted as red spheres. Putative interactions are shown as dotted lines, the gray lines showing interactions behind other residues. Interactions with residues via backbone interactions are denoted with an asterisk. Bond lengths and specific interactions are described in the text. The figure was generated using Pymol (*35*).

binds on a millisecond time scale by the use of stopped-flow spectroscopy. In this study, we are monitoring changes that occur after NADP$^+$ has already bound. It is clear there is a relatively slow phase relating to a conformational change of FMN and/or protein structure indicating a multistep mechanism.[2] The principal component of fluorescence emission on ligand binding is attributed to the FMN domain (*24*), and studies with the isolated FAD/NADPH domain indicated that the fluorescence emission intensity was 13-fold reduced compared with that of nNOS$_{RED}$, consistent with previous studies (*24*). For the related protein NADPH-cytochrome P450 reductase, Narayanasami et al. have shown that increased flavin fluorescence is associated with increased solvent exposure (*36*). The fluorescence changes on ligand binding were qualitatively similar for CaM-bound and CaM-free enzyme, with the large fluorescence quench accompanying binding of the natural substrate NADP$^+$ (Figure 2). The progressive removal of binding determinants through the use of (i) NADP$^+$ fragments or (ii) the alternative coenzyme NAD$^+$ in binding studies led to less extensive fluorescence emission quenching of the flavin cofactors (Figure 2). Fluorescence quenching studies shown in Figure 2 are for substrate and/or fragment concentrations at 10 times the K_i value measured during steady-state turnover studies of enzyme inhibition (Table 1). Combined, the data reveal that a number of the key interactions made between substrate and protein are required to elicit a substantial decrease in flavin fluorescence and, in particular, the fluorescence emission of the FMN cofactor. The data suggest that the binding of NADP$^+$ effects a local change in the environment of the FMN cofactor, consistent with the FMN domain occupying a different conformation. Chaotropes have been shown to increase the intensity of the 530 nm peak as the protein is unfolded or denatured and FMN becomes more exposed to the solvent (*37*, *38*). The loss in intensity upon addition of coenzyme fragments might indicate that the FMN domain becomes less solvent exposed, consistent with the domain shuffle hypothesis proposed by Garcin and co-workers (*26*). The most significant loss of intensity is due to the presence of NADP$^+$, the natural substrate. It would appear that while in steady-state studies 2′,5′-ADP is as good as an inhibitor of electron transfer as NADP$^+$, it is not as good at effecting FMN mobility since the decrease in fluorescence is only ~55% of that of NADP$^+$. The combination of the 2′- and 5′-phosphates of 2′,5′-ADP is clearly much better at inducing a decrease in fluorescence compared to either 2′-AMP or 5′-AMP alone. The loss of fluorescence using 2′-AMP is ~45% of that with NADP$^+$, and 2′-AMP is much better alone than 5′-AMP, which decreases fluorescence by only ~27% compared to that observed with NADP$^+$. NMN results in a loss of fluorescence intensity of only ~10% of that for NADP$^+$, which is most probably a result of having no significant interactions with the nNOS$_{RED}$ protein environment. Strangely, NAD$^+$ is worse at effecting a fluorescence decrease than is NMN, despite having multiple interactions with the protein. From this evidence, it would appear that the 2′-phosphates are a key to invoking FMN mobility in the nNOS$_{RED}$ oxidized state as NAD$^+$ shares many of the other key interactions with NADP$^+$ within the enzyme. It would appear that FMN mobility is tuned to NADP$^+$ and that the presence of the NMN moiety in NADP$^+$ is required to facilitate the largest decrease in fluorescence, and therefore the greatest mobility, despite the NMN moiety apparently having no interactions with the enzyme, as determined from the crystal structure described above. The

[2] Although not observed on relatively fast time scales in stopped-flow studies, where NOS is mixed with ligand, these conformational equilibria, attained after several minutes, are likely to be relevant to the functioning of NOS in vivo where the enzyme and ligand are pre-equilibrated.

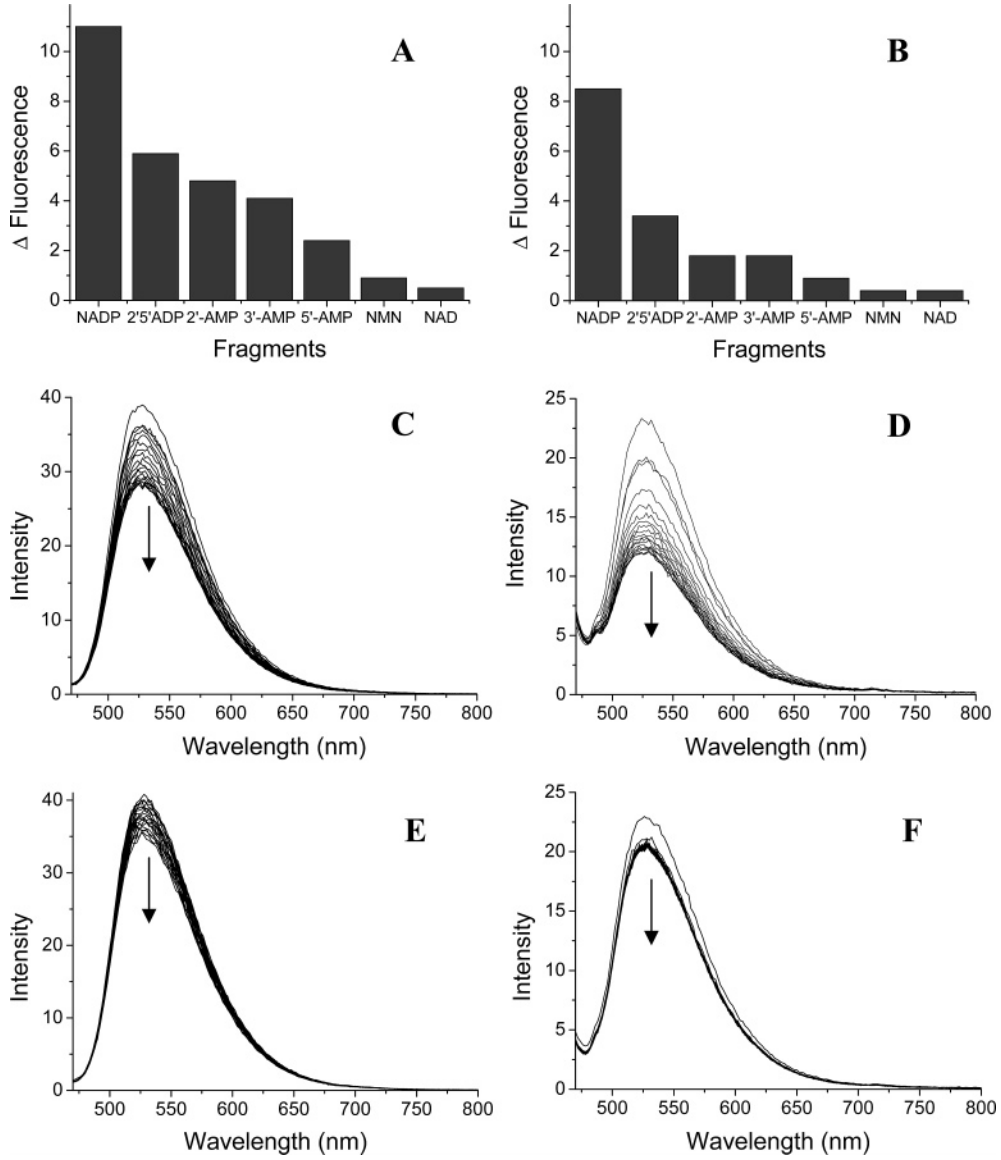

FIGURE 2: Time-dependent fluorescence changes following incubation of $nNOS_{RED}$ with $NADP^+$, analogues, and structural fragments. (A) Histogram illustrating the extent of the end point decrease in absolute fluorescence emission for CaM-bound $nNOS_{RED}$ at 530 nm following incubation of $nNOS_{RED}$ with $NADP^+$ and its analogues and fragments for 20 min, as described in Materials and Methods. (B) As for panel A, but with $nNOS_{RED}$ in the absence of CaM. (C) Time-dependent changes in fluorescence emission upon incubation of CaM-bound $nNOS_{RED}$ with $NADP^+$. (D) As for panel C, but with $nNOS_{RED}$ in the absence of CaM. (E) Time-dependent changes in fluorescence emission upon incubation of CaM-bound $nNOS_{RED}$ with 2′,5′-ADP as a ligand. (F) As for panel E, but with $nNOS_{RED}$ in the absence of CaM. Conditions: 25 °C in 100 mM Tris-HCl (pH 7.4) and 10% (v/v) glycerol. nNOS CaM^+ contained 1 mM $CaCl_2$, while CaM^- contained 1 mM EGTA. nNOS reductase (4 μM) was mixed with substrate (2′-AMP, 3′-AMP, 5′-AMP, 2′,5′-ADP, NMN, $NADP^+$, or NAD^+) at 10 times the K_i, and the subsequent change in fluorescence was monitored over the range of 470−800 nm from an excitation wavelength of 453 nm. Maximum fluorescence emission is observed at 530 nm. Selected fluorescence spectra are shown over the collection period (20 min) with the final (lowest) spectrum shown being the end point spectrum.

conformational freedom of the FMN domain is consistent with the domain shuffle hypothesis for electron transfer in $nNOS_{RED}$, which requires a mobile FMN domain to shuttle electrons between the FAD cofactor and the oxygenase domain in the second subunit.

Electron Paramagnetic Resonance Spectroscopy. The EPR spectrum of one-electron-reduced $nNOS_{RED}$ in the presence of CaM (Figure 3a) shows the single-line EPR spectrum with a ΔH_{ptp} of 19.8 G and a g of 2.0038, typical of a neutral flavosemiquinone radical (*39*). In the absence of CaM (Figure 3b), this signal is unperturbed, showing that the presence of CaM alone does not influence flavosemiquinone formation in the unliganded, one-electron-reduced state. However, in the presence of CaM and $NADP^+$, the double integral of the EPR signal (proportional to the number of unpaired electrons contributing to the signal) is reduced by 70% and the ΔH_{ptp} is reduced to 16.6 G, with the g value constant at 2.0038. These parameters are somewhat equivocal, with the line width suggestive of an anionic flavosemiquinone (*39*), while the g value indicates that the neutral flavosemiquinone has been maintained [in flavoenzymes that can form both neutral and anionic flavosemiquinones, formation of the latter is normally associated with a decrease in the g value (*40*)]. Therefore, this species could be an anionic flavosemiquinone in an unusual environment or a neutral flavosemiquinone radical with a novel unpaired electron spin density distribution. The line widths of flavosemiquinone radical EPR spectra are determined by hyperfine coupling between the

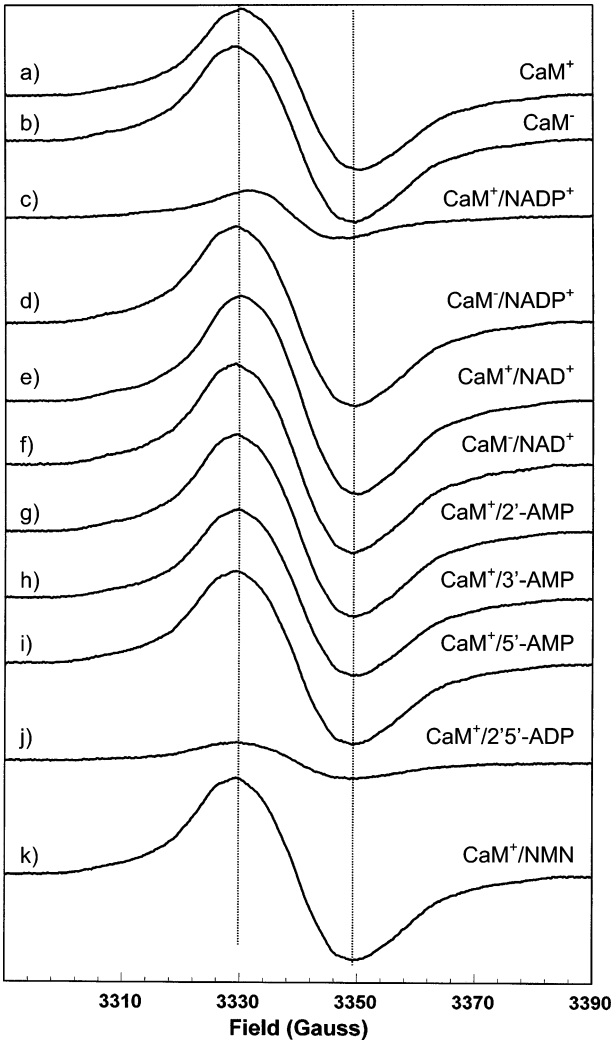

FIGURE 3: EPR spectra for $nNOS_{RED}$ in the one-electron-reduced state in the presence of $NADP^+$, analogues, and nucleotide fragments. Spectra were recorded both in the absence of the effector calmodulin (CaM^-) and in its presence (CaM^+). Experimental conditions: microwave power of 10 μW (determined through the use of saturation curves to be the highest nonsaturating power possible for these samples in our spectrometer), modulation frequency of 100 kHz, modulation amplitude of 1 G, and temperature of 70 K. The protein concentration was 112 μM. All ligands were added at 10 times the respective K_i value (as shown in Table 1). The flavosemiquinone yield was estimated to be 0.37−0.40 equiv in all samples except those giving rise to spectra c and j, wherein it was approximately 0.10 and 0.12 equiv, respectively.

unpaired electron of the radical state and magnetic nuclei (protons and nitrogen atoms) attached to the cofactor. A change in the distribution of the unpaired electron over the flavosemiquinone and/or the loss of a proton through ionization results in a change in spectrum line width due to the effect on the hyperfine coupling (*41*). Therefore, the binding of $NADP^+$ modifies the environment of the FMN cofactor in two ways. First, the yield of flavosemiquinone is reduced, presumably through modification of the E_M for the cofactor, and second the environment is perturbed in a way that modifies the distribution of the unpaired electron within the flavosemiquinone that is formed. Remarkably, in the absence of CaM (Figure 3d), the spectrum appears as in the unliganded state. Perhaps as remarkably, NAD^+ gives rise to the same spectrum as the unliganded state in the presence and absence of CaM (Figure 3e,f) as do the nucleotide fragments 2′-ADP, 3′-ADP, and 5′-ADP (Figure 3h−j). This clearly suggests that phosphate groups at the 2′- and 5′-positions, as in $NADP^+$, are key to the effect observed in Figure 3c. When the nucleotide fragment 2′,5′-ADP is bound to the enzyme, the 70% reduction in intensity observed in the $NADP^+$-bound state is again observed, but this time without the modification of ΔH_{ptp} observed with $NADP^+$, showing that the neutral flavosemiquinone form observed in the unliganded enzyme is maintained. This clearly separates the two effects. The presence of the 2′- and 5′-phosphate groups is required for the modification in flavosemiquinone yield and, therefore presumably, E_M, and the effect is clearly cooperative with two phosphate groups having a much larger effect than either does in isolation. However, the effect on the line width (ΔH_{ptp}) of the flavosemiquinone signal requires the presence of the nicotinamide half of $NADP^+$. This suggests that the use of NMN might invoke the change in ΔH_{ptp} without the decrease in flavosemiquinone yield. However, Figure 3k clearly shows that this is not the case and that the line width change is specific for the full $NADP^+$ molecule. Therefore, these ligand binding studies show a modification of the environment of the flavosemiquinone that occurs specifically in the presence of $NADP^+$ and CaM. The effect is synergistic, requiring both phosphorylation of the adenosine portion and the presence of the nicotinamide portion of the substrate. This environment change results in both a change in the E_M of the FMN cofactor and a change in the electronic structure of the flavosemiquinone state. This is in complete agreement with the steady-state fluorescence studies, in which both 2′,5′-ADP and $NADP^+$ have significant effects on the flavin environments, with $NADP^+$ having the greater effect. Thus, both the fluorescence and EPR studies show that the FMN cofactor is affected by the binding of substrate and that this effect is transmitted by the protein, probably involving residues such as Arg-1400 which interacts with the 2′-phosphate group of $NADP^+$. The functional significance of such behavior within the domain shuffle model is clear, supporting the selective modification of the FMN environment through domain motion in the presence of CaM and the physiological reductant.

Potentiometric Analysis of the Flavin Cofactors Using UV−Visible Spectroscopy and EPR. Previous potentiometric studies of the FAD and FMN flavins of the neuronal NOS reductase domain suggested that the binding of the effector molecule CaM did not result in significant alterations to the reduction potentials of either flavin (*26*). In view of studies reported in this paper and previously, which indicate conformational change induced on binding of CaM and alteration in the environment(s) of the flavins, we re-determined the reduction potentials of the flavin cofactors in the neuronal NOS reductase in the presence and absence of CaM. In these experiments, we undertook both spectroelectrochemical measurements under strict anaerobic conditions (Figure 4) and measurements of flavin radical content by EPR redox titration. Redox titrations were conducted in Tris-HCl buffer rather than in potassium phosphate, to ensure that Ca^{2+} ions required for binding of CaM to the protein are not sequestered by phosphate ions to form an insoluble complex. The ability of CaM to stimulate reductase activity (cytochrome *c* reduction) was demonstrated in the nNOS reductase

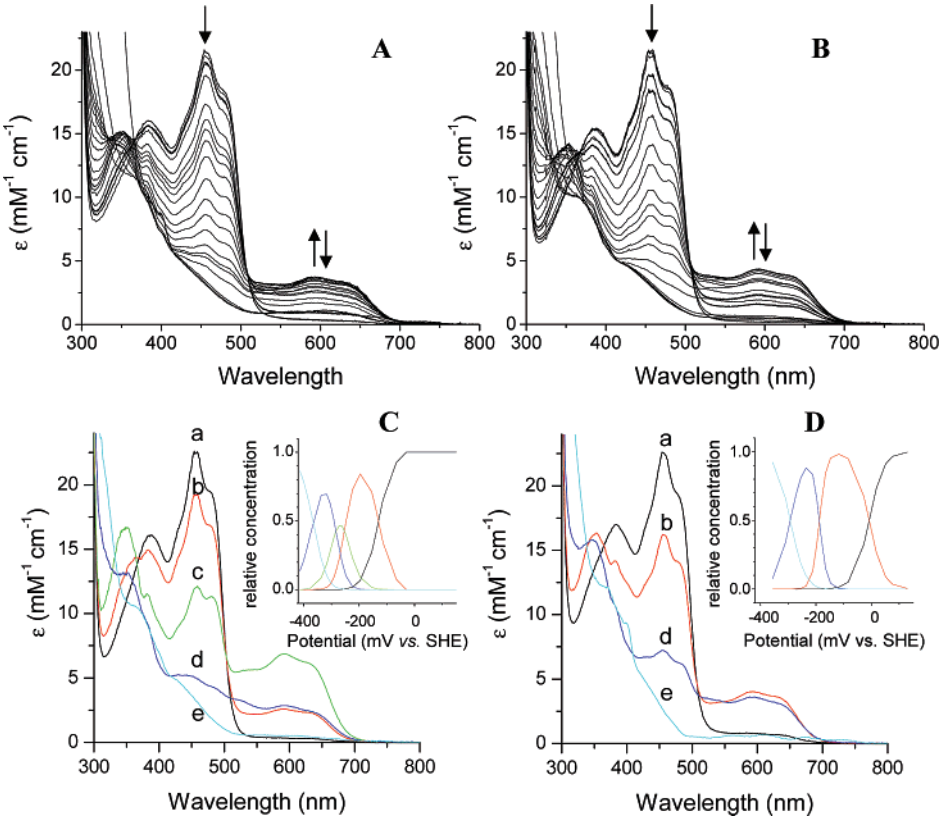

FIGURE 4: UV−visible absorption spectra collected during spectroelectrochemical titrations of the calmodulin-free (CaM^-) and calmodulin-bound (CaM^+) forms of $nNOS_{RED}$. Extinction coefficients are shown for the enzymes. Approximately 20 μM enzyme was used in each titration. Arrows indicate the direction of absorption change at key wavelengths during the reductive phase of the redox titrations. (A and C) $nNOS_{RED}$ CaM^+ titration. (B and D) $nNOS_{RED}$ CaM-free titration. Panels C and D show the deconvoluted spectra of the (a) oxidized, (b) one-electron-reduced, (c) two-electron-reduced, (d) three-electron-reduced, and (e) four-electron-reduced enzymes, determined by global analysis of the data in panels A and B as described in Materials and Methods. The colors are carried throughout the panels, and the insets show the concentration profiles of each species as a function of potential. Species c was not resolved from the CaM-free data. Experimental conditions: anaerobic titrations using 100 mM Tris-HCl buffer (pH 7.4) and 10% (v/v) glycerol at 25 °C, containing mediators as described in Materials and Methods. Coefficients for absorption of each deconvoluted spectral species are 22.5 and 0.3 mM^{-1} cm^{-1} (at 456 and 592 nm, respectively) for species a, 19.2 and 2.6 mM^{-1} cm^{-1} for species b, 12.0 and 6.8 mM^{-1} cm^{-1} for species c, 5.0 and 2.9 mM^{-1} cm^{-1} for species d, and 3.2 and 0.5 mM^{-1} cm^{-1} for species e for the CaM^+ form. Comparable values are 22.5 and 0.8 mM^{-1} cm^{-1} for species a, 16.2 and 4.0 mM^{-1} cm^{-1} for species b, 7.2 and 3.6 mM^{-1} cm^{-1} for species d, and 2.6 and 0.6 mM^{-1} cm^{-1} for species e for the CaM^- form.

enzyme preparations used for these studies to confirm the reported behavior of the CaM-bound form (*20*, *30*−*32*).

The data fits from spectroelectrochemical studies are generally in good agreement with those from EPR-based methods and indicate that a considerable change in redox properties of the nNOS flavins is observed upon binding of calmodulin (see Table 2 for data sets from optical titrations). For the CaM-free form of nNOS reductase, the flavin potentials are rather different from those previously reported for the enzyme. The FMN couples are both more positive (by ∼55 and 68 mV from data at 456 nm) than previously reported, although the separation between the oxidized−semiquinone and semiquinone−hydroquinone couples of the FMN is not greatly different from previous studies of the CaM-free nNOS FMN (approximately −212 mV vs −225 mV) (*27*). The FAD oxidized−semiquinone potential is also rather more positive than previously reported (approximately −172 mV vs −232 mV) in the CaM-free enzyme. However, the FAD values reported here are more similar to those we have reported previously for the isolated FAD domain of nNOS (−177 and −310 mV for the FAD domain vs −172 and −288 mV reported here from CaM-free nNOS reductase) (*42*). When CaM binds, there is a substantial shift in the flavin potentials, as observed in either of the plots of absorption versus applied potential at 592 nm (at the flavin blue semiquinone maximum) and ∼456 nm (at the peak absorption for the oxidized nNOS reductase, Figure 5A). The oxidized−semiquinone and semiquinone−hydroquinone couples of the FMN are both shifted considerably to more negative values (by ∼144 and ∼86 mV, respectively), and there is also some alteration in the potential of the FAD, with both the oxidized−semiquinone (by ∼64 mV) and semiquinone−hydroquinone (by ∼14 mV) couples becoming rather more negative on CaM binding. While the fitting required regimes (multiple redox couples and absorption coefficients as variables) are complex, the fitting processes for the absorption versus potential data are somewhat simplified by the fact that (as previously described) an isosbestic point for the oxidized−semiquinone couple of both flavins is located at ∼507 nm, enabling initital estimates of the semiquinone−reduced couples of the FMN and FAD to be obtained by data fitting at this wavelength. Similarly, an isosbestic point for the semiquinone−hydroquinone transition is located at ∼416 nm, and initial estimates of the reciprocal couples can be obtained from data fitting at this wavelength. Inputting the values determined from data fitting

Table 2: Midpoint Potentials (millivolts vs the standard hydrogen electrode) for the Four-Electron Reduction of $nNOS_{RED}$ Obtained by Fitting eqs 1 and 2 to Absorbance vs Potential Data Derived from Spectroelectrochemical Redox Titrations at Near-Maximal Wavelengths for Absorption of the Oxidized Flavoenzymes (456 nm) and for the Neutral Blue Semiquinone Form of the Flavins (592 nm), Respectively[a]

		FMN		FAD	
		E_1'	E_2'	E_1'	E_2'
CaM^-	A_{456}	6 ± 7	-206 ± 8	-172 ± 8	-288 ± 10
	A_{592}	14 ± 8	-197 ± 10	-176 ± 10	-290 ± 8
	global analysis	-9 ± 5	-199 ± 2		-292 ± 5
	EPR	-24 ± 5	-182 ± 9	-167 ± 10	-284 ± 3
CaM^+	A_{456}	-138 ± 5	-292 ± 8	-236 ± 7	-302 ± 10
	A_{592}	-134 ± 5	-293 ± 12	-246 ± 10	-305 ± 8
	global analysis	-130 ± 8	-284 ± 10	-254 ± 10	less than -300[b]
	EPR	-158 ± 4	-278 ± 27	-268 ± 34	-281 ± 32

[a] E_1' and E_2' are the midpoint potentials for the oxidized−semiquinone and semiquinone−reduced forms of the flavins, respectively. Redox titrations were performed in the absence (CaM^-) and presence (CaM^+) of calmodulin. Global analysis of the optical potentiometry data was performed with Specfit/32 as described in Materials and Methods. The FMN^- and FAD^- species (c in Figure 4C) were not resolved from the CaM^- data, and the quoted potential for FMN E_2'/FAD E_1' was determined from a single two-electron step from species b to species d. The EPR data (Figure 5B) were fitted using eq 3. Potentiometric experiments were performed on four different enzyme preparations, while the EPR studies were performed on two separate enzyme preparations. [b] Deconvolution of the spectrum of the four-electron-reduced species is complicated by the proximity and similarity of the E_2' FMN, E_1' FAD, and E_2' FAD potentials for the CaM^+ enzyme. For this reason, we are less confident in the value of the E_2' FAD potential (-360 ± 10 mV) determined by global analysis (for this data set) than in the other potentials that are given.

at isosbestic points as initial estimates for data fitting at 456 and 592 nm expedites the fitting process and the convergence of parameters to produce the final data sets presented in Table 2.

While the extent of the change in the reduction potentials of the flavins induced by CaM binding is clearly obvious from the major shift in the applied potential required to initiate reduction of the more positive potential flavin (the FMN, >100 mV) (Figure 5A), we sought independent verification of the induced shift in potential through spectroscopic redox titration by EPR. Since EPR spectroscopy detects only the paramagnetic flavosemiquinone state of the flavin cofactors, it can be used to determine the potentials for the FMN and FAD cofactors through quantitation of the flavosemiquinone with changes in applied potential. An additional advantage of the EPR approach is the relative simplicity of the spectrum (see Figure 3) which, being a single line arising from only the flavosemiquinone state, is much less complex than the optical spectrum that exhibits bands arising from all three oxidation states of the flavin. However, EPR measurements are made on frozen solutions and thus require anaerobic preparation of several different enzyme samples at different levels of reduction, and the freezing of these samples in liquid nitrogen prior to analysis by EPR. As can be seen in Figure 5B, the substantial CaM-induced shift in flavin potentials determined from UV−visible potentiometry is confirmed from EPR redox titration. In particular, the large CaM-induced negative shifts in FMN potentials are obvious from EPR analysis (Figure 5B).

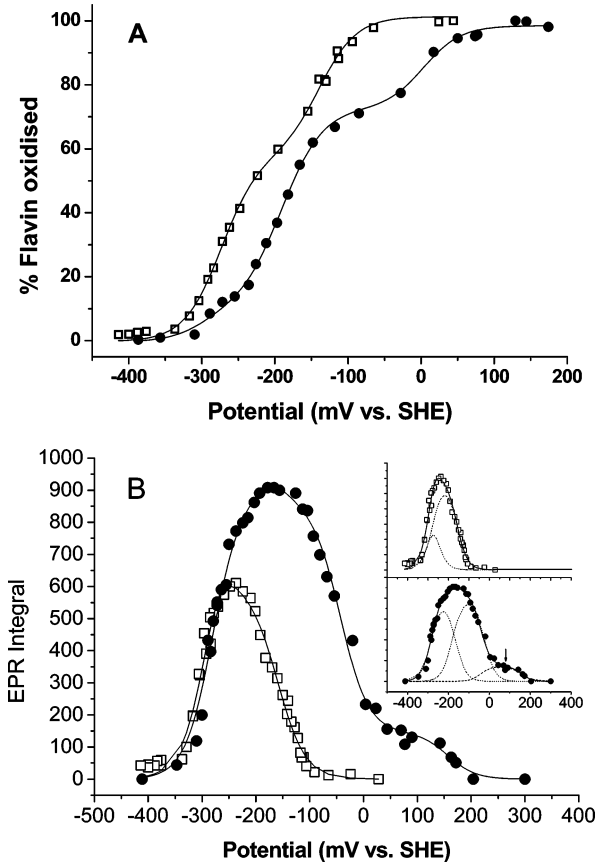

FIGURE 5: Redox titration data from spectroelectrochemical titrations (A) and from EPR (B). Panel A shows absorption data at 456 nm for the calmodulin-free [CaM^- (●)] and calmodulin-bound [CaM^+ (□)] forms of $nNOS_{RED}$ plotted vs applied potential. Titration data are fitted to eq 1, as described in the text. Panel B shows the relative integral of the flavosemiquinone EPR spectrum plotted vs applied potential. The maximum flavosemiquinone yield amounted to 0.82 equiv in the presence of CaM and 1.18 equiv in its absence. Titration data that are shown were fitted to eq 3 (describing a 2 × 2 one-electron reduction process) for the CaM-bound enzyme. Filled circles represent data for CaM^- enzymes and empty squares data for CaM^+ enzymes in both cases. The inset shows the individual contribution from the FMN and FAD redox couples to the total EPR integral. The CaM^- data show an additional species centered at ~100 mV (marked with an arrow). These data were fitted with an additional term described in Materials and Methods, with an E_5' of 157 mV and an E_6' of −42 mV and an apparent concentration of $17 \pm 4\%$ of the enzyme concentration.

An important observation from the EPR data (Figure 5B) is that the peak quantity of flavosemiquinone accumulated is substantially greater for the titration of the CaM-free form than for the CaM-bound species, as would be expected for the greater separation between the redox couples of the individual flavins in the CaM-free enzyme ($\Delta E_1/E_2$ for FMN of 212 mV and for FAD of 116 mV) compared to the CaM-bound enzyme (154 and 66 mV, respectively). This is apparent upon comparison of the maximum relative concentration of the semiquinone species determined from global analysis of the optical redox titrations described below (insets of Figure 4C,D). In optical titrations, although a substantial shift in potentials is obvious from even qualitative analysis of the absorption versus potential data (see Figure 5A), there is apparently only an up to ~15% increase in the maximum A_{592} accumulated in the CaM-free enzyme over the CaM-bound form (Figure 4). EPR analysis of the same samples

used in optical redox titrations confirms that the maximal amount of flavosemiquinone present is actually substantially greater in the CaM-free enzyme than is suggested from A_{592}.[3] To strengthen this point, we performed redox titrations on CaM$^{\pm}$ nNOS in the presence of 2′,5′-ADP, which mimics the effect of NADP$^+$, but is non-redox active. The data from this titration (for publication at a later date) show clearly that the amount of semiquinone at equilibrium is substantially smaller in the 2′,5′-ADP complex, thus supporting the conclusions from the EPR studies.

In addition to fitting data at individual wavelengths, we have employed global analysis to simultaneously fit data at all wavelengths and deconvolute the spectra of each reduced species. The values in Table 2 show good correlation between the midpoint potentials calculated using the Nernst equation at various wavelengths and global analysis. The only exception is the CaM-bound E_2' of FAD which is ~60 mV lower in the global analysis fitting than in fitting to the Nernst equations. We are unclear as to exactly why this is, but it may result from difficulty in deconvoluting the spectra of the fully reduced (four-electron) species.

With respect to the fitting of the data for the EPR in Figure 5B, there are issues relating to how the data can be fitted. The function used to fit these data recognizes that there is both an increase and a decrease in EPR intensity due to formation and then reduction of the radical. The function also recognizes that the EPR versus potential plot described here should take the form of two superimposed bell-shaped curves according to the redox transitions of the two flavins (deconvoluted in the inset of Figure 5B). Accurate fitting of the CaM-free data requires an additional term to describe the "bump" at ~100 mV (marked with an arrow in the inset of Figure 5B). This additional species has a much lower concentration than the enzyme (17 ± 4% relative) and is assigned to one or more mediators used to expedite electronic equilibration of the enzyme during the redox titration. In this respect, hydroxynaphthoquinone and phenazine methosulfate undergo some reduction in this part of the titration. Absorption spectra are largely unaffected by contributions from these molecules, but they clearly can contribute to the EPR spectrum to a small extent.[4] That the EPR data as fitted are consistent with the data from optical titrations gives further confidence to the fact that there is a substantial alteration in flavin potentials on CaM binding. Minor features discerned in the EPR titration cannot be accurately fitted to appropriate functions without simultaneously distorting the entire potential series and indicating completely unrealistic parameters for the transitions. The slightly greater "scatter" in points on the EPR curves likely results from the greater level of processing for these samples, but data otherwise are completely consistent with those from optical titrations.

In conclusion, our potentiometric analysis of the CaM-bound and CaM-free forms of neuronal NOS reductase domains indicates clearly that there is a major shift in the thermodynamic properties of the flavins (and particularly the FMN) induced on binding the effector protein calmodulin.[5] Although this is in contrast to an earlier report (*27*), it should be noted that proteins used for assays reported here were purified in Tris-HCl buffer and in the presence of Ca^{2+} and were thus replete with these ions on addition of CaM protein, allowing full binding of the protein as verified by fluorimetric and enzyme assays. The shift in redox potential is also consistent with the environmental changes expected for nNOS flavins on association of CaM (*26*). It is important to emphasize the differences in the experimental conditions used to purify nNOS by ourselves and previous groups (*27*, *43*). In the work of both Noble et al. (*27*) and Gao et al. (*42*), EDTA is present in all purification buffers. We have shown (*23*) that the presence of EDTA removes CaM from NOS but, more importantly, leads to a proteolyzed form of the enzyme. Noble and co-workers (*27*) add excess CaM after purification to overcome this, but as the enzyme is proteolyzed, CaM may bind in a different fashion, if at all, to that in the unproteolyzed form. While we are not directly questioning the results of these previous studies, we feel that their method of purification raises questions about the outcome of their experiments. In fact, our data for the CaM$^-$ redox titrations are in relatively close agreement with the previous findings. This supports our idea that this is the first potentiometric study in which we are truly measuring the effect of CaM on flavin reduction since we are sure we have nNOS reductase in both the CaM-bound and CaM-free forms. Repeat titrations have been performed on different batches of purified nNOS reductase and give reproducible results.

To further prove the reproducibility of our findings, we have taken CaM$^+$ nNOS reductase and titrated it with dithionite under strictly anaerobic conditions until it is fully reduced. Solid anaerobic EGTA was then added to the sample to a final concentration of 2 mM to chelate any Ca^{2+} in the solution and so dissociate CaM. After passing through a filter within the glovebox to remove any precipitated Ca-EGTA and particulate matter, the sample was then reoxidized with potassium ferricyanide. Reduction potentials and UV−vis spectra over the range of 300−800 nm were recorded at multiple points of reduction and/or oxidation. Data (Figure S1 of the Supporting Information) reproduce those obtained

[3] The data from EPR potentiometric analysis are entirely consistent with the data from optical analysis, demonstrating that there is a substantial shift in flavin potentials mediated by the binding of CaM. We cannot be certain of the origins of the differences seen in the EPR and optical spectra. Possible explanations include freezing-induced effects that differ between the forms or spin−spin interactions that perturb signal intensities. It must be stressed that these phenomena relate only to the magnitude of the signals and do not otherwise affect the fitting of data that gives rise to the cited midpoint potentials. The symmetrical nature of the EPR data makes precise evaluation of the EPR couples more error prone than for the UV−visible potential data. This is reflected in the errors listed in Table 1.

[4] If this feature were due to one of the flavin semiquinones, this would indicate that the FAD populates spectacularly more semiquinone than does the FMN (which is at odds with what is known about the thermodynamic properties of the flavins in the enzyme). Additionally, the remaining data are only adequately fitted when two redox couples are included, consistent with the FMN and FAD semiquinone species.

[5] Electron transfer is relatively slow in NOS compared with expected intrinsic rates ($>10^8$ s^{-1}) of electron transfer over the relatively small distance observed in the crystal structure of nNOS reductase (*26*). We infer that electron transfer is limited by conformational change of the protein, as is often the case with dynamic "modular" electron transfer proteins (e.g., see ref *44* for a recent review), a proposition that is consistent with the domain shuffle hypothesis proposed by Garcin et al. (*26*). Perturbations in the thermodynamic driving force of the magnitude identified in our work should not affect the *observed* rate of electron transfer since the overall rate is controlled by the conformational change.

for separate samples of CaM^+ and CaM^- enzyme. Performing these titrations on a single sample and imitating our findings clearly show that we are able to control the binding and dissociation of CaM from nNOS reductase.

These results show that CaM not only has a "secondary" effect on the protein structure, allowing for subsequent binding of a specific ligand to perturb the redox potentials of the FMN cofactor as shown in Figure 3, but also has a "primary" and specific effect on the protein, leading to a change in flavin cofactor redox potentials. That these effects are evident even though FAD and FMN cofactors are found on separate domains of $nNOS_{RED}$ indicates the structural complexity of the interaction between nNOS and CaM. The negative shifts in the FMN redox couples on CaM binding are also likely to favor electron transfer between FMN (at least from the FMN hydroquinone form) and the NOS heme iron, where the potential of the nNOS heme iron in complex with L-arginine has been reported to be −316 mV in the absence of substrate and −306 and −278 mV in presence of L-arginine and *N*-hydroxy-L-arginine, respectively (*41*). From values reported here, the FMN semiquinone−hydroquinone couple decreases from approximately −206 to approximately −292 mV upon CaM binding, and thus, CaM binding leads to the transfer of electrons from FMN hydroquinone to heme iron, being thermodynamically more favorable in the presence of substrate. This may be a further advantageous effect of CaM binding that assists in expediting NOS catalysis.

Concluding Remarks. Our studies provide evidence of the conformational change associated with the FMN domain in neuronal NOS reductase and indicate ligand-induced effects on its relative conformation. Mapping of key interactions between nicotinamide coenzymes and fragments thereof is apparent both in the fluorescence emission of the flavin cofactors and in EPR spectra of the FMN flavosemiquinone state. The reported solution studies are entirely consistent with ligand−protein interactions observed in the crystal structure of the reductase domain of nNOS (*26*). Using both EPR and optical spectroscopy methods, and despite dogma based on spectroelectrochemical titrations alone (*27*), we have demonstrated a substantial calmodulin-dependent perturbation in the midpoint reduction potentials of the flavins using both EPR and UV−visible potentiometric methods. Moreover, binding of 2′,5′-ADP and $NADP^+$ effects a perturbation in the midpoint reduction potentials of the enzyme-bound flavin(s) which leads to relative destabilization of flavin semiquinone compared with ligand-free (i.e., coenzyme fragment-free) forms of the enzyme. Our studies support a model of electron transfer, inferred from the "static" X-ray crystal structure of nNOS reductase (*24*), which invokes FMN domain mobility and is triggered by Ca^{2+} calmodulin binding and antagonized by substrate binding.

SUPPORTING INFORMATION AVAILABLE

Additional spectroelectrochemical titration data for the calmodulin-bound and calmodulin-free forms of nNOS reductase. This material is available free of charge via the Internet at http://pubs.acs.org.

REFERENCES

1. Schmidt, H. H., and Walter, U. (1994) NO at work, *Cell 78*, 919−925.
2. Chiueh, C. C., Hong, J.-S., and Leong, S. K. (2002) Nitric Oxide: Novel Actions, Deleterious Effects, and Clinical Potential, *Ann. N.Y. Acad. Sci. 962*, 1−437.
3. Garthwaite, J., Charles, S. L., and Chess-Williams, R. (1988) Endothelium-derived relaxing factor release on activation of NMDA receptors suggests role as intercellular messenger in the brain, *Nature 336*, 385−388.
4. Ignarro, L. J., Buga, G. M., Wood, K. S., Byrns, R. E., and Chaudhuri, G. (1987) Endothelium-derived relaxing factor produced and released from artery and vein is nitric oxide, *Proc. Natl. Acad. Sci. U.S.A. 84*, 9265−9269.
5. Palmer, R. M., Ferrige, A. G., and Moncada, S. (1987) Nitric oxide release accounts for the biological activity of endothelium-derived relaxing factor, *Nature 327*, 524−526.
6. Bredt, D. S., and Snyder, S. H. (1994) Nitric oxide: A physiologic messenger molecule, *Annu. Rev. Biochem. 63*, 175−195.
7. Griffith, O. W., and Stuehr, D. J. (1995) Nitric oxide synthases: Properties and catalytic mechanism, *Annu. Rev. Physiol. 57*, 707−736.
8. Marletta, M. A. (1993) Nitric oxide synthase structure and mechanism, *J. Biol. Chem. 268*, 12231−12234.
9. Stuehr, D. J. (1997) Structure-function aspects in the nitric oxide synthases, *Annu. Rev. Physiol. 37*, 339−359.
10. Bredt, D. S., Hwang, P. M., Glatt, C. E., Lowenstein, C., Reed, R. R., and Snyder, S. H. (1991) Cloned and expressed nitric oxide synthase structurally resembles cytochrome P-450 reductase, *Nature 351*, 714−718.
11. Wang, M., Roberts, D. L., Paschke, R., Shea, T. M., Masters, B. S., and Kim, J. J. (1997) Three-dimensional structure of NADPH-cytochrome P450 reductase: Prototype for FMN- and FAD-containing enzymes, *Proc. Natl. Acad. Sci. U.S.A. 94*, 8411−8416.
12. Leclerc, D., Wilson, A., Dumas, R., Gafuik, C., Song, D., Watkins, D., Heng, H. H.., Rommens, J. M., Scherer, S. W., Rosenblatt, D. S., and Gravel, R. A. (1998) Cloning and mapping of a cDNA for methionine synthase reductase, a flavoprotein defective in patients with homocystinuria, *Proc. Natl. Acad. Sci. U.S.A. 95*, 3059−3064.
13. Paine, M. J., Garner, A. P., Powell, D., Sibbald, J., Sales, M., Pratt, N., Smith, T., Tew, D. G., and Wolf, C. R. (2000) Cloning and characterization of a novel human dual flavin reductase, *J. Biol. Chem. 275*, 1471−1478.
14. McMillan, K., and Masters, B. S. S. (1995) Prokaryotic expression of the heme- and flavin-binding domains of rat neuronal nitric oxide synthase as distinct polypeptides: Identification of the heme-binding proximal thiolate ligand as cysteine-415, *Biochemistry 34*, 3686−3693.
15. Cho, H. J., Xie, Q. W., Calaycay, J., Mumford, R. A., Swiderek, K. M., Lee, T. D., and Nathan, C. (1992) Calmodulin is a subunit of nitric oxide synthase from macrophages, *J. Exp. Med. 176*, 599−604.
16. Daff, S., Sagami, I., and Shimizu, T. (1999) The 42-amino acid insert in the FMN domain of neuronal nitric-oxide synthase exerts control over Ca^{2+}/calmodulin-dependent electron transfer, *J. Biol. Chem. 274*, 30589−30595.
17. Abu-Soud, H., and Stuehr, D. (1993) Nitric oxide synthases reveal a role for calmodulin in controlling electron transfer, *Proc. Natl. Acad. Sci. U.S.A. 90*, 10769−10772.
18. Sheta, E. A., McMillan, K., and Masters, B. S. S. (1994) Evidence for a bidomain structure of constitutive cerebellar nitric oxide synthase, *J. Biol. Chem. 269*, 15147−15153.
19. Craig, D. H., Chapman, S. K., and Daff, S. (2002) Calmodulin activates electron transfer through neuronal nitric-oxide synthase reductase domain by releasing an NADPH-dependent conformational lock, *J. Biol. Chem. 277*, 33987−33994.
20. Abu-Soud, H. M., Yoho, L. L., and Stuehr, D. J. (1994) Calmodulin controls neuronal nitric-oxide synthase by a dual mechanism. Activation of intra- and interdomain electron transfer, *J. Biol. Chem. 269*, 32047−32050.
21. Matsuda, H., and Iyanagi, T. (1999) Calmodulin activates intramolecular electron transfer between the two flavins of neuronal nitric oxide synthase flavin domain, *Biochim. Biophys. Acta 1473*, 345−355.
22. Matsuda, H., Kimura, S., and Iyanagi, T. (1999) Calmodulin activates intramolecular electron transfer between the two flavins of neuronal nitric oxide synthase reductase domain, in *Flavins and Flavoproteins* (Ghisla, S., Kroneck, P., Macheroux, P., and Sund, H., Eds.) pp 171−174, Weber, Berlin.
23. Knight, K., and Scrutton, N. S. (2002) Stopped-flow kinetic studies of electron transfer in the reductase domain of neuronal nitric oxide

synthase: Re-evaluation of the kinetic mechanism reveals new enzyme intermediates and variation with cytochrome P450 reductase, *Biochem. J. 367*, 19−30.
24. Gachhui, R., Presta, A., Bentley, D. F., AbuSoud, H. M., McArthur, R., Brudvig, G., Ghosh, D. K., and Stuehr, D. J. (1996) Characterization of the reductase domain of rat neuronal nitric oxide synthase generated in the methylotrophic yeast *Pichia pastoris*. Calmodulin response is complete within the reductase domain itself, *J. Biol. Chem. 271*, 20594−20602.
25. Zhang, J., Martasek, P., Paschke, R., Shea, T., Masters, B. S. S., and Kim, J. P. (2001) Crystal structure of the FAD/NADPH-binding domain of rat neuronal nitric-oxide synthase: Comparisons with NADPH-cytochrome P450 oxidoreductase, *J. Biol. Chem. 276*, 37506−37513.
26. Garcin, E. D., Bruns, C. M., Lloyd, S. J., Hosfield, D. J., Tiso, M., Gachhui, R., Stuehr, D., Tainer, J. J. A., and Getzoff, E. D. (2004) Structural basis for isozyme-specific regulation of electron transfer in nitric-oxide synthase, *J. Biol. Chem. 279*, 37918−37927.
27. Noble, M. A., Munro, A. W., Rivers, S. L., Robledo, L., Daff, S. N., Yellowlees, L. J., Shimizu, T., Sagami, I., Guillemette, J. G., and Chapman, S. K. (1999) Potentiometric analysis of the flavin cofactors of neuronal nitric oxide synthase, *Biochemistry 38*, 16413−16418.
28. Daff, S., Sharp, R. E., Short, D. M., Bell, C., White, P., Manson, F. D. C., Reid, G. A., and Chapman, S. K. (1996) Interaction of cytochrome c with flavocytochrome b_2, *Biochemistry 35*, 6351−6357.
29. Nishida, C. R., and de Montellano, P. R. O. (1998) Electron transfer and catalytic activity of nitric oxide synthases. Chimeric constructs of the neuronal, inducible, and endothelial isoforms, *J. Biol. Chem. 273*, 5566−5571.
30. Wolthers, K. R., and Schimerlik, M. I. (2001) Reaction of neuronal nitric-oxide synthase with 2,6-dichloroindolphenol and cytochrome c^{3+}: Influence of the electron acceptor and binding of Ca^{2+}-activated calmodulin on the kinetic mechanism, *Biochemistry 40*, 4722−4737.
31. Dixon, M. (1953) The determination of enzyme inhibitor constants, *Biochem. J. 55*, 170−171.
32. Dutton, P. L. (1978) Redox potentiometry: Determination of midpoint potentials of oxidation-reduction components of biological electron-transfer systems, *Methods Enzymol. 54*, 411−435.
33. Munro, A. W., Noble, M. A., Robledo, L., Daff, S. N., and Chapman, S. K. (2001) Determination of the redox properties of human NADPH-cytochrome P450 reductase, *Biochemistry 40*, 1956−1963.
34. Tiso, M., Konas, D. W., Sharma, M., Garcin, E. D., Getzoff, E. D., and Stuehr, D. J. (2004) Mutagensis of Arg-1400 in neuronal nitric oxide synthase, *FASEB J. 18*, C283−C284.
35. DeLano, W. L. (2002) *The PyMOL Molecular Graphics System*, DeLano Scientific, San Carlos, CA.
36. Narayanasami, R., Horowitz, P. M., and Masters, B. S. S. (1995) Flavin-binding and protein structural integrity studies on NADPH-cytochrome P450 reductase are consistent with the presence of distinct domains, *Arch. Biochem. Biophys. 316*, 267−274.
37. Adak, S., Ghosh, S., Abu-Soud, H. M., and Stuehr, D. J. (1999) Role of reductase domain cluster 1 acidic residues in neuronal nitric-oxide synthase. Characterization of the FMN-FREE enzyme, *J. Biol. Chem. 274*, 22313−22320.
38. Narayanasami, R., Nishimura, J. S., McMillan, K., Roman, L. J., Shea, T. M., Robida, A. M., Horowitz, P. M., and Masters, B. S. S. (1997) The influence of chaotropic reagents on neuronal nitric oxide synthase and its flavoprotein module. Urea and guanidine hydrochloride stimulate NADPH-cytochrome c reductase activity of both proteins, *Nitric Oxide 1*, 39−49.
39. Palmer, G., Müller, F., and Massey, V. (1971) Electron paramagnetic resonance studies on flavoprotein radicals, in *Flavins and Flavoproteins*, University Park Press, Baltimore.
40. Eriksson, L. E., and Ehrenberg, A. (1973) Powder ESR and ENDOR spectra of flavoprotein radicals, *Biochim. Biophys. Acta 295*, 57−66.
41. Ost, T. W., and Daff, S. (2005) Thermodynamic and kinetic analysis of the nitrosyl, carbonyl, and dioxy heme complexes of neuronal nitric-oxide synthase. The roles of substrate and tetrahydrobiopterin in oxygen activation, *J. Biol. Chem. 280*, 965−973.
42. Dunford, A. J., Marshall, K. R., Munro, A. W., and Scrutton, N. S. (2004) Thermodynamic and kinetic analysis of the isolated FAD domain of rat neuronal nitric oxide synthase altered in the region of the FAD shielding residue Phe1395, *Eur. J. Biochem. 271*, 2548−2560.
43. Gao, Y. T., Smith, S. M. E., Weinberg, J. B., Montgomery, H. J., Newman, E., Guillemette, J. G., Ghosh, D. K., Roman, L., Martasek, J. P., and Salerno, J. C. (2004) Thermodynamics of oxidation-reduction reactions in mammalian nitric-oxide synthase isoforms, *J. Biol. Chem. 279*, 18759−18766.
44. Leys, D., and Scrutton, N. S. (2004) Electrical circuitry in biology: Emerging principles from protein structure, *Curr. Opin. Struct. Biol. 14*, 642−647.

BI7001339